

# Molecular Rayleigh scattering to measure fluctuations in density in low speed heated wind tunnel flows

J. Panda\*, NASA Ames Research Center, Moffett Field, CA  
S. D. Schery, Aerospace Computing Inc., Mountain View, CA

## Abstract

**A Rayleigh scattering based density-fluctuations measurement system has been setup inside a low-speed wind tunnel of NASA Ames Research Center. The immediate goal of the test has been to study transition on a heated flat plate. At first a smaller scale setup was created around a small low-speed heated jet, and then the setup was modified for use in a wind tunnel. The paper discusses means of overcoming various difficulties associated with particle cleaning, vibration isolation and stray light reduction to obtain a cleaner signature of the Rayleigh scattered light. A two-PMT cross-correlation system and photo-electron counting processes were used to minimize the shot noise floor in the spectra of turbulent density fluctuations. Preliminary results from both setups are presented. It was found that a signal-to-noise ratio of  $10^2$  to  $10^4$  was achievable with increasing plume/plate temperature.**

## I. INTRODUCTION

Measurement of turbulent fluctuations spectra in high speed and/or heated flows, especially across shock-waves, is extremely difficult using the current experimental techniques. Tools, such as particle image velocimetry, and intrusive probes, cannot measure spectra of scalar fluctuations. We have started an effort to develop a particle-free, non-intrusive, molecular Rayleigh scattering based technique to simultaneously measure density and velocity fluctuations for wind tunnel applications. There exist multiple obstacles on the way, and the present work, directed at using a demonstration unit in a low-speed research tunnel, attempts to find the means to overcome some of these obstacles and to provide a stepping stone for larger applications.

The molecular Rayleigh scattering technique provides a fundamental way of measuring flow properties of gases: bulk density via measuring molecular number density, bulk velocity via measuring the central peak in the distribution of molecular speed, and temperature via measuring the full-width at half-maxima of that distribution. The technique has been used extensively in supersonic free-jets<sup>1,2,3</sup> and pre-

mixed combustions flows<sup>4,5</sup>, and has provided unprecedented insight into unsteadiness of shock structure, fluctuations responsible for sound radiation, behavior of combustion process, and modeling constants for CFD simulations. Typically, a narrow-line-width laser beam is passed through the wind tunnel test section, and light scattered by oxygen and nitrogen molecules from a small region (probe volume) on the beam is collected and spectrally resolved. A measure of the Doppler shift and its spectral broadening provide data for the velocity and temperature while total scattered intensity provides determination of density. Analysis of the optical spectrum over small time intervals provides time histories of the fluctuations. The fluctuation in air density is determined by monitoring the intensity variations of the scattered light.

Since the information is obtained directly from the molecular behavior of the gas flow, without the introduction of seed particles or any other additives, it is the source of both the strengths and the difficulties of this technique. The Rayleigh scattered light can be easily overwhelmed by Mie scattered light from the naturally present dust particles in the air. There were many efforts in the past where a Rayleigh system was setup around small laboratory jets. However, the next step of creating a similar setup around larger scale test facilities was fraught with many new challenges. Past successes for jet noise studies<sup>1,2</sup> were due to effective means of removing particles from the primary jet as well as the entrained air, and a lay-out of the optical system that minimized the effect of vibration. However, all of these applications involved open jets where the confinements of a wind tunnel were absent. Wind tunnel environments provide additional significant challenges for insertion of the laser beam, containment of specular and diffused reflection, and adequate vibration isolation; also the issue of dust particles looms large. The objective of the present work is to overcome each of the above difficulties for a setup in a small, low-speed wind tunnel. The immediate goal is to measure density fluctuations over 0-10kHz bandwidth in boundary-layer and wake flows. Eventually, the setup will be extended to measure velocity and temperature.

---

\*Associate Fellow, AIAA

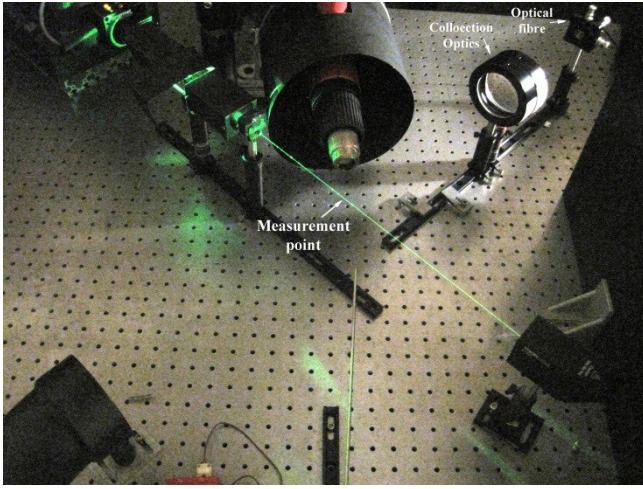


**Figure 1** Photograph of the Rayleigh setup to measure turbulent fluctuations in a heated jet.

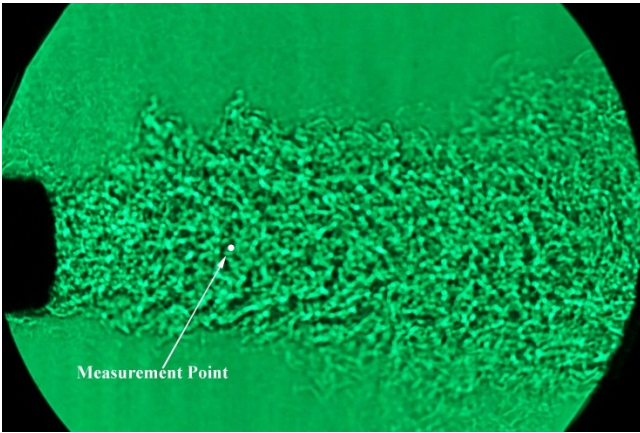


**Figure 2** Shadowgraph of a heated jet surrounded by an 8'' diameter low-speed, dust-free stream.

### A. Laser Rayleigh scattering:

When a laser beam is allowed to pass through a gas, the molecules present cause inelastic and elastic light scattering. The inelastic part is called Raman scattering and the elastic part as Rayleigh scattering. The Raman scattering cross-section is far weaker than that of Rayleigh; typically for room temperature nitrogen, vibrational and rotational Raman scattering contribute, respectively, 0.1% and 1% of the total scattered light. Therefore, the elastic Rayleigh scattering process describes most of the scattered light. For gas density measurement, variation of the total light intensity with the molecular number density is of interest. Since this variation is identical for both Rayleigh and Raman scattering process, a separation between the two is unnecessary. The following considers the Rayleigh scattered part where the scattered light,  $P_s$ , collected from a probe volume,  $V_{sc}$  into a solid angle,  $d\Omega$ , can be written as the following<sup>6</sup>.

$$P_s = m I_0 V_{sc} \left( \sum_i \mu_i \sigma_i \right) \sin^2 \chi \Omega = k' m \quad (1)$$

Here  $m$  is the molecular number density,  $I_0$  is the incident light intensity,  $\sigma_i$  is the Rayleigh scattering cross-section of the species  $i$  in the gas mixture,  $\mu_i$  is the mole fraction of species  $i$ , and  $\chi$  is the angle between the incident electric vector and the direction of light collection. The Rayleigh scattering cross-section depends on the refractive index of the particular species and is constant for a fixed wavelength laser and a fixed gas mixture (air for this work). For a fixed optical setup, the scattered laser power is directly proportional to the molecular number density. Now, the number density  $m$ , is related to the bulk density,  $\rho$  through the following:

$$m = \frac{\rho N_A}{M}, \quad (2)$$

where  $M$  is the molecular weight and  $N_A$  is the Avogadro constant ( $6.022 \times 10^{26} \text{ kmole}^{-1}$ ). The scattered light intensity was measured using a photomultiplier tube and a photon counting process was performed. The number of photons collected during a fixed time interval  $\Delta t$  can be written as:

$$N = \frac{\varepsilon P_s \Delta t}{h \nu} = \frac{\varepsilon \rho N_A I_0 V_{sc} \left( \sum_i \mu_i \sigma_i \right) \sin^2 \chi \Omega \Delta t}{M h \nu} \quad (3)$$

$$= k \rho \Delta t$$

where,  $h$  is the Planck constant,  $\nu$  is the frequency of the laser light and  $\varepsilon$  is the overall collection efficiency (a product of the light transmission efficiency and the quantum efficiency of the photomultiplier tube). Equation 3 shows that the photon count over a fixed time interval is directly proportional to the gas density at the probe volume. The proportionality constant  $k$  has to be determined through a calibration process. The advantage of the photon counting approach over the conventional measurement of analog PMT output<sup>4</sup> is a clearer estimate of measurement uncertainty due to electronic shot noise. A commercially available, PC-based, multi-scalar counter was used for this purpose. The multi-scalar allowed for photo-electron counting over 262,144 contiguous time bins of user-specified time duration.

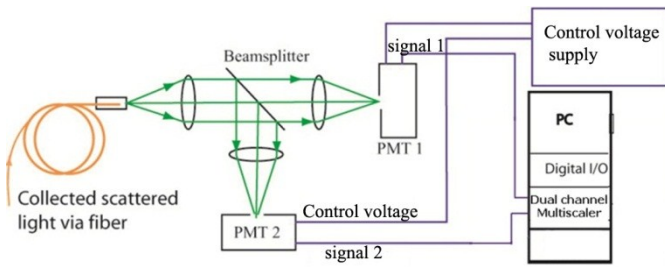


**Figure 3.** Dual PMT setup to measure fluctuations in Rayleigh scattered light.

## II. EXPERIMENTAL SETUP

The present effort is the first attempt to set up a Rayleigh scattering based aerodynamic measurement system at NASA Ames. First a large set of optics and optoelectronic components were identified and purchased. Then individual components were tested, and finally the optical system was setup.

### A. Setup around a hot, low speed air jet:

A 22mm diameter hot air plume was created using electrical heaters that can produce hot plumes in the temperature range of ambient to 250°C. A critical

element, as mentioned earlier, is to minimize the effect of dust particles. An air cleaning system, consisting of a blower and a HEPA® filtering system was installed (not shown in fig 1) to produce a 200mm diameter, clean co-flowing stream of air around the hot plume. The heater intake for the hot-plume also used this clean air to minimize contamination by dust particles. Figure 2 shows a shadowgraph of the hot jet produced from this facility.

The central element of the optical setup (Figure 1) was a continuous wave (CW) laser beam that passed through the hot plume. The 532 nm, continuous wave, single mode, incident laser beam for the optical setup was produced from a frequency-doubled, Nd:VO<sub>3</sub> solid state source that emitted a maximum of 2W power. The laser beam was focused to a 0.15mm waist at the probe volume. The molecular scattered light from a small region on the beam was collected and measured using Photo-multiplier tubes (PMT). The collection optics was made of a pair of 75mm diameter achromatic lens that focused the scattered light on a multi-mode optical fiber.

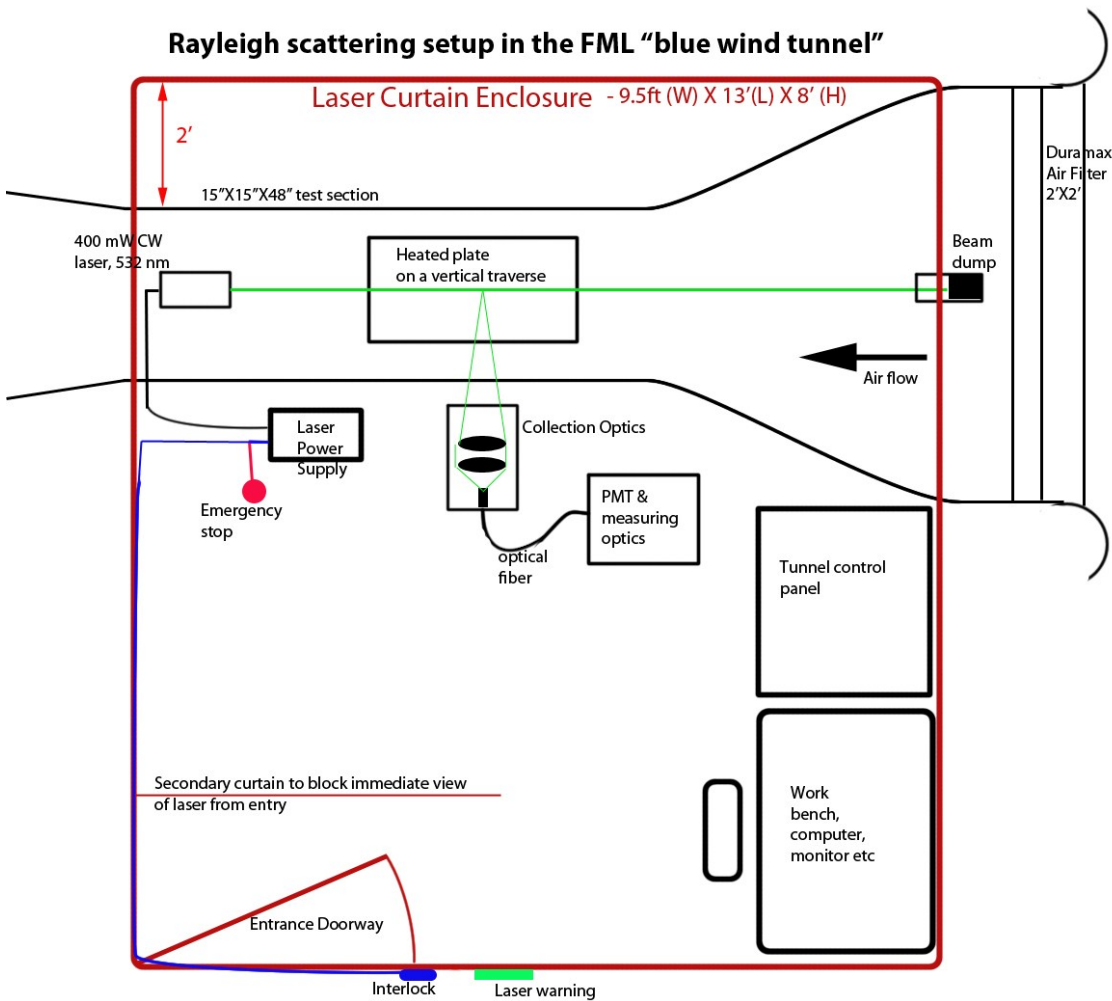


**Figure 4** Rayleigh scattering setup in a low speed wind tunnel.

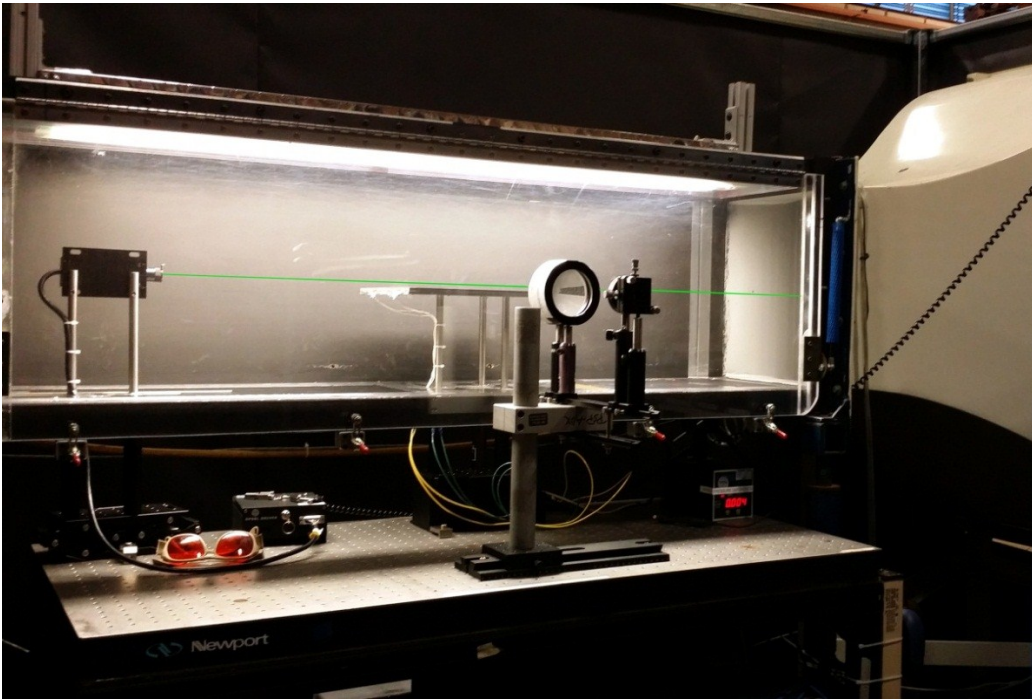


**Figure 5** Photograph of the Rayleigh setup

The fiber core diameter of 0.4mm, and the 1.5 magnification ratio of the collection lens, fixed the length of the probe volume to 0.6 mm. The setup was for a point measurement inside the plume. The scattered light, collected by the receiving fiber, was transmitted to a separate set of optics (fig. 3), where it was collimated and then split into two equal parts by a thin-film beam splitter. Each of the beams was refocused into individual photomultiplier tubes. Photon counting electronics were then used to measure light intensities.

#### **B. Setup in a low-speed wind tunnel:**

After evaluating a series of small wind tunnels at NASA Ames, it was finally decided to create this setup around a low-speed, in-draft tunnel (“blue” tunnel) that provided the necessary ease of access and ease of modifications. Air flow in the velocity range of 0-150ft/s through the 15”X15”X48” test section was created by a variable speed blower which sucked ambient air through a 4’X4’ inlet section, a series of turbulence management screens, and a 1:10.24 area contraction section (fig. 4). The test article was a pair of 12” (length) X 9” (width) flat plates that sandwiched a 1kW electrical strip heater. Layers of fiber glass insulation were placed between the heater and the bottom plate to reduce heat loss through the bottom surface. The strip heaters were connected to a variable voltage AC power supply that heated the top plate at a wide range of temperature. The plate was traversed vertically for boundary layer survey, using an automated traversing stage. The top surface was painted flat black with high temperature spray paint to minimize stray

scattering especially when the laser beam was brought very close to the plate surface.

A different, small profile, laser light source (than that used for the heated plume facility described earlier) had to be used for various reasons. A large lasing head is obviously unsuitable for placement inside a test section. Use of mirrors to transfer light in the test section would have involved some scattering from the reflective surfaces. Such scatterings would have increased the level of background illuminations and reduced the signal to noise ratio. Therefore a small size (1.78”X1.38”X5.54” size head mounted on a 0.4” thick X 2.32” wide heat sink), solid-state, diode-pumped, laser source was selected that produced linearly polarized (100:1 polarization ratio), 400mW of power at 532nm wavelength. The laser was oriented for maximum scattering intensity towards the collection direction. The beam diameter was 1.2mm. The laser source was mounted downstream of the test article, and the beam passed parallel to the heated plate. The beam was ultimately terminated upstream, in a small-profile beam-dump placed ahead of the wind tunnel contraction section. The wake from the beam-dump and its mount was expected to be dissipated inside the long contraction section.

The optics to collect Rayleigh scattered light was the same one used in the heated jet facility, and described earlier. Therefore the length of the probe volume was 0.6mm as before. The collection optics was oriented at 90° to the laser beam and was placed outside the test section on an optical bread board. The bread board also held the laser source and the heated plate. The

dual-PMT setup for measuring the intensity of scattered light was also transferred from the plume facility.

An 8-foot tall laser-curtain enclosure was built around test section as shown in figure 4 for the safe operation of the optical system. Two cutouts were made on two sides of the enclosure for the wind tunnel structures to pass through. The entrance door of this enclosure was interlocked.

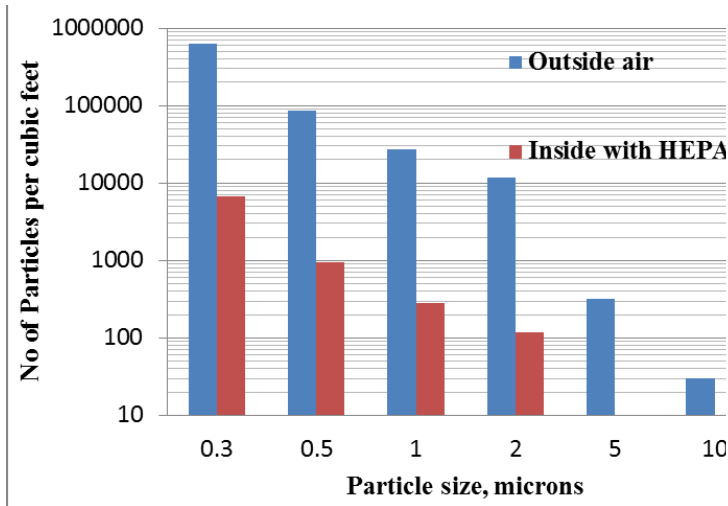


**Figure 6** Effectiveness of HEPA filter in reducing dust particles in the wind tunnel facility.

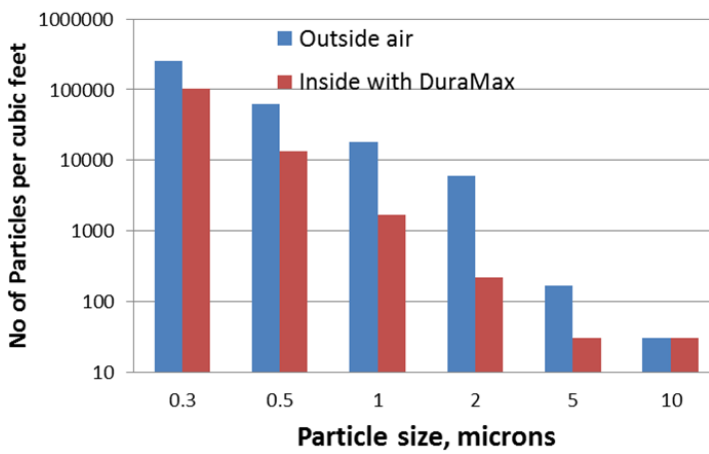


**Figure 7** Effectiveness of 95% efficient Duramax filter in reducing dust particles in the wind tunnel facility.

*Air Filtration system:* Any practical application of the Rayleigh scattering technique requires multiple strategies to minimize the effect of Mie scattering from aerosol particles naturally present in the air stream. A two prong approach was undertaken: (a) a hardware approach of thorough cleaning of the air stream; and (b) a software approach of identification and removal of the signature from the passage of dust particles.

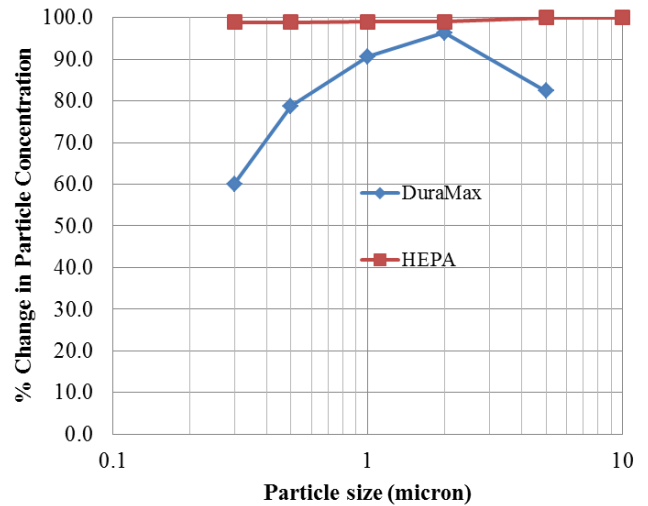


**Figure 8** Comparison of filtration efficiency between two types of filters.

*Cleaning of the air stream:* The concentration of the dust particles in the air-stream was studied systematically, and progressive improvements were made over time. At first, the particle content in the ambient and inside the wind tunnel, in the size range of 0.3micron to 10micron, was measured with an aerosol counter. It was found that the existing coarse filter hardly reduced the particle counts inside the stream. This pointed to the need of using better air filters. Additionally the wind tunnel screens and the wall-surfaces were thoroughly cleaned of the dust particles that accumulated over many years of operation (some from the use of particle based techniques). In the next step better air filters were placed at the inlet. Typically air filters that provide increased cleaning also cause a larger pressure drop and restrict air flow. The latter is specified as the allowable maximum velocity on the filter inlet. For example a maximum allowable face velocity of 15 ft/s leads to a maximum test section velocity of roughly 150 ft/s. A means to overcome this limitation is to build a larger air intake chamber around the wind tunnel inlet. However, the goal of the experiment was to reach a maximum of 100 ft/s speed, and therefore no additional chamber was built. Nonetheless, at first a lower 95% filtration efficiency air filter was used, and then a 99.9% HEPA filter was used. Comparisons of particle counts and filtration efficiencies achieved with these two different filters are shown in Figures 6, 7 and 8. Note that in the absence of the filters there were little difference in the particle counts between the test section and the outside ambient air. Compared to the lower efficiency filter, the HEPA filter restricted the maximum allowable flow rate by nearly 15%; still it was chosen for significantly lowering the aerosol concentration in the test section. It's worth noting that the particle count in the ambient air in the urban area where NASA Ames center is located is dependent on the

level of pollution and other factors. In a clear winter day, after a rainstorm, the particle counts could be lower by a factor of 20 compared to that in a highly polluted day.

The use of the HEPA filter is expected to minimize impact of this variation.

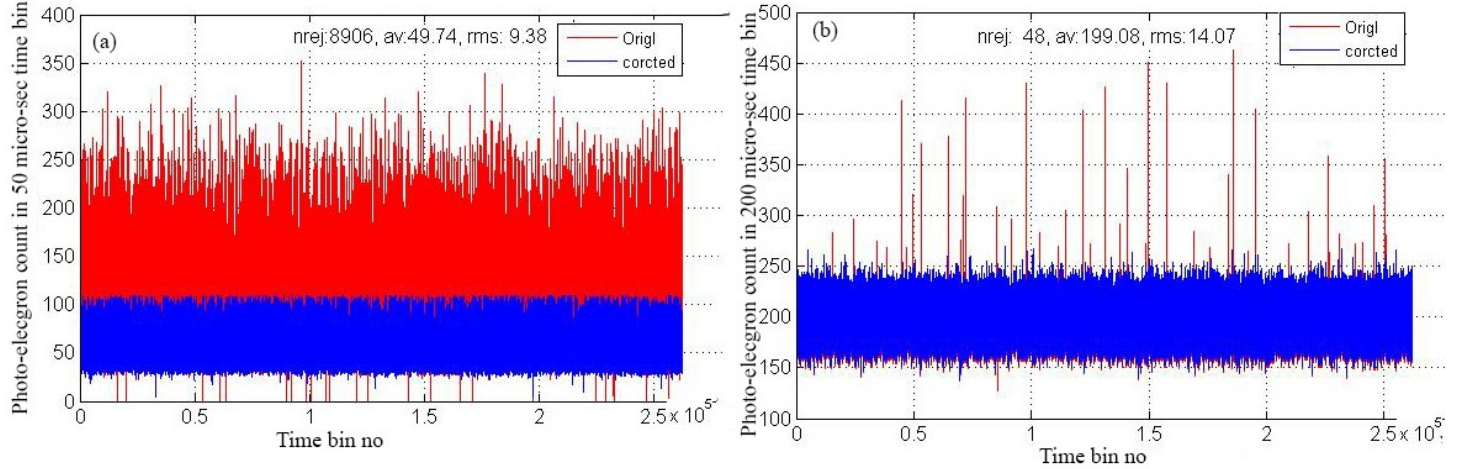


**Figure 9** Time traces of photo-electron count before and after software cleaning when (a) the lower efficiency filter was used (b) the higher efficiency HEPA filter was used.

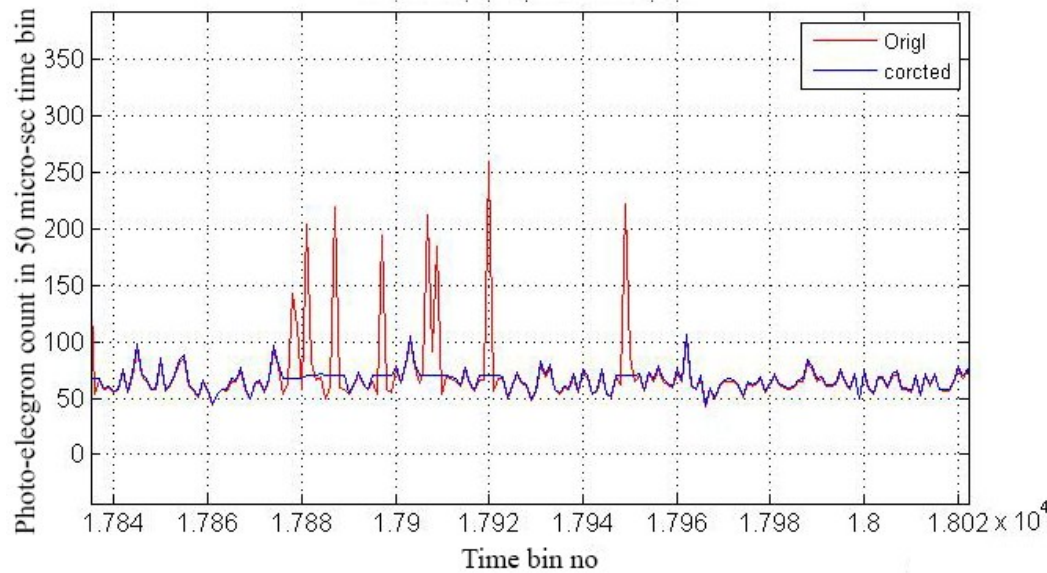


**Figure 10** Software removal of particle signature from time trace of photo-electron count (zoomed-in view of a small section of data shown in fig. 9a).

*Software approach of cleaning particle trace:* The passage of particles was accompanied by a sharp rise in the count rate. As mentioned earlier, the present setup uses photo-electron count in contiguous series of time bins. Figure 9 shows two such time series obtained using two different air filters. Photo-electron count follows Poisson’s statistics, therefore, even when there is no variation in light intensity the count rate fluctuates within a limit. The passage of particles created a far larger swing. A close up view of a small region in one of the time traces is shown in figure 10. Data points where the count rate was larger than five times the standard deviation were replaced by the average count:

$$\text{If } N_i \geq kN_{stddev} \quad N_i = N_{av}, \quad k = 5 \quad (4)$$

The blue lines in figures 9 and 10 were obtained by this means. Although mostly successful, a drawback of this process is that the relatively weaker signature from smaller particles, or particles passing through the outskirts of the Gaussian laser beam could not be removed. This was found to increase the noise floor of the spectrum calculated from the time trace. Nevertheless, it was nearly impossible to remove all dust particles in a wind tunnel flow, and when the numbers of dust particles were few, the peak stripping technique was effective.

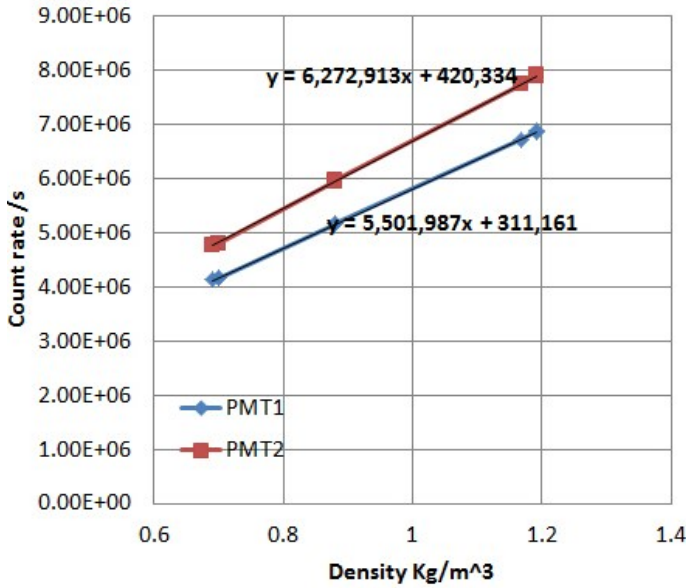


**Figure 11.** Calibration of the Rayleigh scattered signal, photoelectron count rate vs. gas density obtained from the heated plume setup.

*Vibration isolation:* The blower in the wind tunnel created vibration that was found to be transmitted to the test section via the metal duct to which the blower inlet was connected, as well as through the ground. An effective solution for ground vibration was obtained by placing the optical components on a pneumatically isolated breadboard support frame. Isolation from vibration of the test section wall was somewhat more difficult. First, the laser source and the test articles were mounted on the isolated breadboard (fig. 5). However, any small contact with the wind tunnel wall was found to vibrate the component. Therefore, holes bigger than the supporting rods, were cut on the tunnel floor. This caused small leakage of air.

### III. RESULTS AND DISCUSSION

#### A. Density calibration

The advantage of the photon counting approach over the conventional measurement of analog PMT output<sup>4</sup> is a clearer estimate of measurement uncertainty due to electronic shot noise. Photoelectron counting ( $N_i$ ,  $i = 0, 1, 2, \dots, n-1$ ) was performed over a large number ( $n = 262,144$ ) of contiguous time bins covering 13s to 52s time duration, depending on the user-selected duration of the individual bins, typically 50-200 micro-sec. The bin duration effectively represented the sampling interval in conventional digital signals<sup>2</sup>. After removing the particle signature (eqn. 4 above), a pulse pile-up correction was made on each data point:

$$\dot{N}_{i-correct} = \dot{N}_{i-meas} / (1 - \Delta t_{pair} \dot{N}_{i-meas}) \quad (5)$$

Here,  $\Delta t_{pair}$  is the minimum time difference between two photo-electron pulses necessary for the counter to distinguish (20ns for the present instrument).

The time average of the counts represented the average intensity of the Rayleigh scattered light from the probe volume. A calibration process was necessary to determine the proportionality constant between the photon count rate and the air density. Figure 11 shows sample calibration curves. To obtain these curves the temperature of the hot plume was varied and the light intensity from the measurement point was measured via series of photo-electron counts. The average air density at the measurement location was determined by measuring local temperature using a thermocouple probe, and by knowing the ambient pressure. Subsequently, a straight line was fitted through the data to determine the proportionality constants  $a$  and  $b$ .

$$N_{av} = (a \rho + b) \Delta t, \quad \text{where } N_{av} = \frac{\sum N_i}{n} \quad (6)$$

The additional constant  $b$  is needed to account for the ambient light and stray scattered laser light. Since two counters were used, two sets of calibration constants  $a_1, b_1$  and  $a_2, b_2$  were calculated. The linearity of the calibration curve provided confidence in the Rayleigh scattering nature of the collected light.

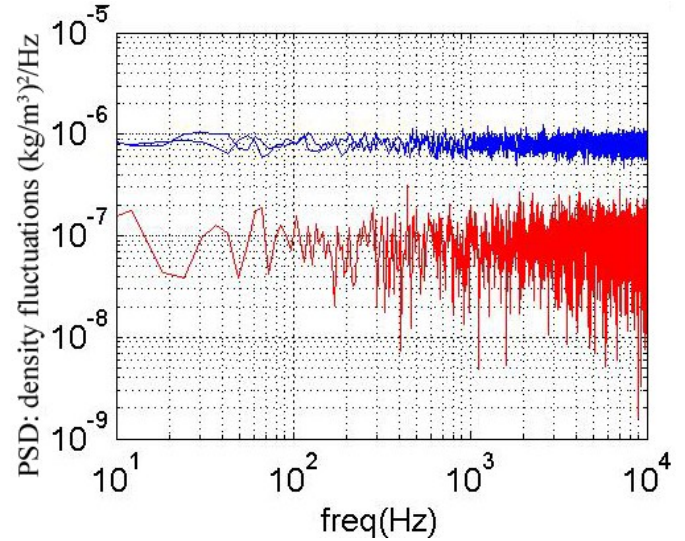


**Figure 12.** Density fluctuations spectra measured from low-speed, unheated plume (without actual air density fluctuation). Blue lines: power spectra of photon counts from individual PMT; red line: cross-spectral density between counts from the two PMT.

#### B. Time average density, density fluctuations spectra, and root-mean-square measurements:

The instantaneous flow density  $\rho$  is divided into a time-averaged part  $\bar{\rho}$ , and a fluctuating part  $\rho'$

$$\rho = \bar{\rho} + \rho' \quad (7)$$

The mean density was related to the average of all bins  $N_{av}$ :

$$\bar{\rho} = \frac{1}{a} \left( \frac{N_{av}}{\Delta t} - b \right) \quad (8)$$

However, the measurement of the fluctuating part was not straightforward, since the electronic shot noise arriving from the photo-multiplier tube needed to be accounted for. Even when the incident light was of constant intensity (no density fluctuation), the rate of photoelectron emission by a PMT showed significant variation referred to as statistical photon count noise or ‘shot-noise’. This noise was random in nature and followed Poisson's statistics. The density fluctuations caused the collected light intensity to vary and the problem became separation of the density fluctuations from the joint statistics of shot-noise and physical light intensity variation. Towards this end a two-PMT cross-correlation procedure was employed<sup>2</sup>.

As mentioned earlier, the collected light was split into two nearly equal parts and measured with two PMTs. The simultaneous photoelectron counting produced two series of data  $N_{1i}$  and  $N_{2i}$  ( $i = 0, 1, 2, \dots, n-1$ ). The average values from each of the time series were subtracted:  $N'_{1i} = N_{1i} - N_{1av}$ ,  $N'_{2i} = N_{2i} - N_{2av}$ , and discrete, one-sided auto-spectra were calculated, which are subsequently multiplied by appropriate calibration constants.

$$\left| P_{N'_i}(f_l) \right| = \frac{2}{n^2} \left| F_{N'_i}(l) \right|^2, \quad (9)$$

$$\text{where, } F_{N'_i}(l) = \sum_{i=0}^{n-1} N'_i \exp \left( j \frac{2\pi i l}{n} \right),$$

$$f_l = \frac{l}{n\Delta t} \quad l = 0, 1, 2, \dots, \frac{n}{2}-1$$

The blue lines in figure 12 shows the auto spectra from an unheated plume where there are no actual density fluctuations. The relatively large energy level in the spectra was entirely due to the electronic shot noise in the photo-electron count. The two series of data was then used to determine one-sided, cross spectral density:

$$\left| P_{N'_1 N'_2}(f_l) \right| = \frac{2}{n^2} \left| F_{N'_1}(l) \cdot F_{N'_2}^*(l) \right|, \quad (10)$$

Superscript \* in the above equation indicates complex conjugate. The density fluctuation spectrum was calculated using appropriate calibration constants  $a_1$  and  $a_2$  for the two photomultiplier tubes:

$$P_{\rho^2}(f_l) = \frac{\left| P_{N'_1 N'_2}(f_l) \right|}{a_1 a_2 (\Delta t)^2} \quad (11)$$

The red line in figure 12 shows the consequence of cross-spectral estimates; the shot noise contribution is reduced by a factor of 10 over the entire spectra. The remaining energy is partially due to insufficient convergence and partially due to the presence of dust particles whose signature could not be completely removed.

The Welch method of modified Periodograms (1967) was used to calculate the auto and cross-spectral density. Each long record was divided into small segments of 4096 data points. The adjacent segments were overlapped by 50%. The modified periodograms of corresponding segments from the two PMTs were calculated and then used to determine local estimates of cross-spectral density. All local estimates were averaged to obtain the final cross-spectral density.

The root-mean-square of the density fluctuations can be calculated by integrating the cross-spectra

$$\rho'_{rms} = \sqrt{\sum_f P_{\rho^2} \Delta f} \quad (12)$$

*Spectra from heated plume:* The cross-spectral procedure (equation 11) was used for the density fluctuations spectra presented in the rest of the paper. Figure 13(a) show a set of power spectra obtained from the probe volume shown earlier in the shadowgraph image of fig 2. Power spectra calculated from different plume temperatures were superimposed; the plot from the unheated jet shows the noise floor in the data. The temperature fluctuation spectra of fig 13(b) were derived assuming pressure fluctuations to be insignificant inside the plume, and  $\rho' T' \ll \rho' \bar{T}$ ,  $T' \bar{\rho}$ , which provides the following relation:

$$P_{T^2}(f_l) = \left( \frac{\bar{T}}{\rho} \right)^2 P_{\rho^2}(f_l) \quad (13)$$

The remarkable aspect of the figure 13 is a demonstration of the wide dynamic range achievable with the setup. The signal to noise floor ratio was  $>10^4$ . The very low speed plume did not have much energy above  $\sim 4$  kHz where the spectral data merged with the noise floor. It is expected that a wider frequency range will be resolved for higher speed flows.

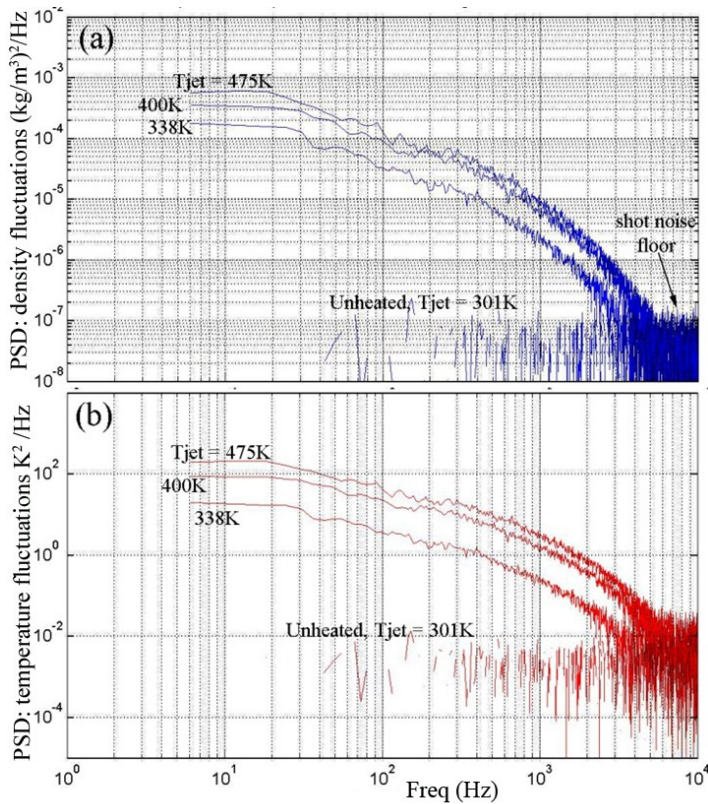


**Figure 13.** (a) Power spectral density (PSD) of air density fluctuations measured from plumes of indicated temperature,  $x/D = 2.5$ ,  $r/D=0$ ; (b) Temperature spectra derived from the density spectra.

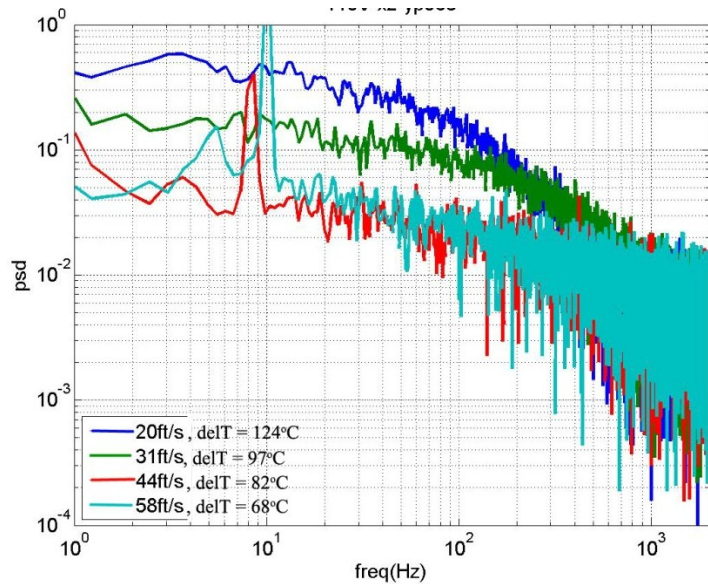


**Figure 14.** Power spectral density (PSD) of air density fluctuations measured from the heated plate with indicated free-stream velocity, and difference of temperature between plate surface and ambient. Probe location  $x=2$ " from leading edge,  $y=0.065$ " from plate surface.

*Spectra from heated plate:* Figure 14 shows sample spectra measured from the temperature boundary layer created on the heated plate in the wind tunnel setup. The extent of temperature rise was relatively lower than that in the hot-plume. Nevertheless, spectral levels were found to rise by a factor of 100 over the noise floor. The sharp peaks at the higher flow speeds were due to the transmission of the tunnel vibration through the mounting rods. This will be minimized in the future work. Also a detailed study of the transition to turbulence will be undertaken.

#### IV. SUMMARY

Considering that this is the first attempt to set up a Rayleigh system at NASA Ames, significant progress has been made in a short time. The present effort started from the very basic step of identifying each optical component, and progressed towards two working setup: around a clean co-flowing hot jet, and in a low-speed wind tunnel. The noticeable aspects of the measured spectra for density fluctuations were the wide frequency range and the high signal to noise ratio that, to the best of our knowledge, no other measurement technique can provide. Multiple obstacles in minimizing aerosol contamination in the air stream, vibration isolation, and suppression of the background scattering had to be overcome to come to this point. Should there be an opportunity for a Rayleigh setup in a larger scale, high-speed, wind tunnel the experience gained from the current effort will be valuable.

#### Acknowledgement

This work was mostly supported by the NASA ARMD seedling fund. The author also acknowledges partial support from the NASA Aeronautical Sciences Project.

#### References

- <sup>1</sup>Panda, J. & Seasholtz, R. G. "Shock structure and shock-vortex interaction in screeching jets measured using Rayleigh scattering," *Physics of Fluids*, vol. **11**, no. 12, 3761-3777, Dec. 1999.
- <sup>2</sup>Panda, J. & Seasholtz, R. G. "Experimental investigation of density fluctuations in high speed jets and correlation with generated noise," *J. Fluid Mech.* **450**, 97-130, 2002.
- <sup>3</sup>Mielke, A. F., Seasholtz, R. G., Elam, K.A., and Panda, J., "Time-average Measurement of Velocity, Density, Temperature, and Turbulence Velocity Fluctuations Using Rayleigh and Mie Scattering," *Exp Fluids*, Vol. **39**, No. 2, 441-454, 2005.
- <sup>4</sup>Pitts, W. M. & Kashiwagi, T., "The application of laser-induced Rayleigh scattering to the study of turbulence mixing," *J. Fluid Mech.* **141**, 391-429, 1984.

<sup>5</sup>Ng, T. T., Cheng, R. K., Robben, F. & Talbot, L.,  
“Combustion-turbulence interaction in the turbulent  
boundary layer over a hot surface,” Lawrence Berkeley  
Laboratory report LBL-13893, Jan. 1982.

<sup>6</sup>Robben, F., “Comparison of Density and Temperature  
Measurement Using Raman Scattering and Rayleigh

Scattering,” Lawrence Berkeley report no: LBL-3294,  
Aug. 1975.

<sup>7</sup>Poggie, J., Erbland, P. J., Smits, A. J. and Miles, R. B.,  
(2004), “Quantitative visualization of compressible  
turbulent shear flows using condensate-enhanced  
Rayleigh scattering,” Experiments in Fluids, 37, 438-  
454, 2004.